

# 3D shape measurement of larger complex objects based on fringe cycle correction

YanJun Fu (伏燕军)\*, Jie Yang (杨杰), Zhigang Wang (王志刚),  
and Haitao Wu (吴海涛)

Key Laboratory of Nondestructive Testing (Ministry of Education), Nanchang Hangkong  
University, Nanchang 330063, China

\*Corresponding author: fyjpkh@sina.com.cn

Received July 4, 2014; accepted September 11, 2014; posted online November 14, 2014

The grating fringe on the reference plane is broadened in the intersecting axis system because of oblique-angle projection. In order to solve this problem, we study the theoretical model of the temporal phase unwrapping method based on the fringe cycle correction. We also study the 3D shape measurement theoretical model of the larger complex objects after considering the coordinate deviation and lens distortion. Experimental results demonstrate that the fringe cycle on the reference plane can be corrected to a constant value, the lens distortion can be corrected, and 3D shape of larger complex objects can be accurately measured.

OCIS codes: 110.6880, 120.2650, 120.2830, 100.5088.

doi: 10.3788/COL201412.121101.

3D shape measurement is very important in both scientific studies and industrial practices<sup>[1]</sup>. Fringe projection profilometry (FPP) has received significant attention for 3D shape measurement because of non-contact operation, full-field acquisition, and fast data processing. According to the spatial position difference between the optical axis of the CCD camera and the projector, FPP can be divided into the intersecting axis system and the parallel axis system. The intersecting axis system is widely used. It consists of two structures, one is the oblique-angle projection of the projector with vertical reception of CCD camera, the other is the oblique-angle reception of CCD camera with vertical projection of the projector. When larger complex objects are measured, both of these structures will have the similar measurement errors. In this letter, the former typical intersecting axis system is discussed. The grating fringe on the reference plane is broadened in the intersecting axis system because of oblique-angle projection, and the fringe cycle is not a constant value. Evident broadening of the fringe cycle causes errors when large objects (1–2 m) are measured, thereby reducing measurement accuracy.

Several researchers have conducted in-depth study of the problem. Sansoni *et al.* pointed out that the cycle of a standard sinusoidal grating projected onto the reference plane is no longer a constant value because of oblique-angle projection, and proposed an error compensation algorithm to correct the error<sup>[2]</sup>. Wang *et al.* obtained the relationship between the virtual reference plane and the reference plane<sup>[3]</sup>. Chen *et al.* not only determined the fringe cycle relationship between the projection plane and the reference plane but also got the phase distribution on the reference plane using the least-squares method<sup>[4]</sup>. Rajoub *et al.* obtained the

relationship of phase-to-height after geometric analysis<sup>[5]</sup>. Luis *et al.* deduced mathematical relationships among projection coordinate, object-coordinate, and camera-coordinate, which did not rely on equivalent wavelength and could remove the measurement error caused by the changes in the equivalent wavelength<sup>[6]</sup>. Wu *et al.* proposed a new method to analyze wrapped phase distribution on a reference plane using static phase measuring profilometry and to modify the projected grating fringe cycle gradually using an iterative algorithm<sup>[7]</sup>. Zhang *et al.* proposed a method to obtain evenly spaced fringes on the reference plane<sup>[8]</sup>, but this method did not build the relationship between coordinates and phases. Cheng *et al.* analyzed the situation of orthographic projection and oblique-angle reception, and obtained the height and height error expressions of the measured object<sup>[9]</sup>. Hao *et al.* analyzed the phase distribution of the  $x$ -axis on the reference plane and phase error. He proposed a method to reduce errors using second-order polynomial fitting<sup>[10]</sup>. Many researchers have conducted studies on lens distortion<sup>[11]</sup>, phase-shifting method<sup>[12,13]</sup>, and calibration<sup>[14–17]</sup>. The methods used to measure complex shape include gray code and phase-shifting methods<sup>[18]</sup>, dual-frequency FPP<sup>[19]</sup>, multi-frequency FPP, etc.. The methods used to measure larger objects include indoor global positioning system, three-coordinate measuring machine, theodolite measuring system<sup>[20]</sup>, optical measurement network<sup>[21]</sup>, etc.

The above-mentioned methods can solve the problem of fringe cycle broadening to a certain extent. However, as the parameters involved usually contain multiple angles, calibration is fairly complex and measurement accuracy is insufficient. Therefore, we propose a 3D shape measurement method based on the fringe cycle correction. The experimental results demonstrated that

the proposed method can solve the problem of the fringe cycle broadening on the reference plane and enables accurate 3D shape measurement of larger complex objects.

Figure 1 shows the measurement system, where  $P$  is the optical center of the projector,  $X$  is the reference plane,  $X'$  is the virtual reference plane, and  $X''$  is the plane of the projector.  $X'$  is perpendicular to the central axis of the projector. The optical axis of the projector and that of the CCD camera intersect at point  $O$ , which is the origin. The optical center of the projector and the optical center of the CCD camera are equidistant from the reference plane, and  $L$  is the value of its distance.  $d$  is the distance between the CCD camera and the projector, and  $f$  is the frequency of the fringe pattern on the reference plane.  $\Delta\varphi$  is the phase difference between the corresponding point on the reference plane and the object. The height of the measured object is<sup>[1]</sup>

$$h = \frac{L\Delta\varphi}{2\pi fd + \Delta\varphi}, \quad (1)$$

where  $L$ ,  $d$ , and  $f$  are obtained by calibration.

Coordinate deviation correction is shown in Fig. 2<sup>[10]</sup>. The image coordinate of point  $E$  is considered the image coordinate of point  $C$  when captured by the CCD camera.  $(X_E, Y_E, Z_E)$  is considered as the coordinate of point  $C$   $(X_C, Y_C, Z_C)$  in the world coordinate system. Thus coordinate deviation occurs. It is very important to correct coordinate deviation when measuring larger objects. According to the corresponding geometry relationship between similar triangles: and consequently,  $(X_C, Y_C, Z_C)$  is the corrected world coordinate of the point  $C$ .

The first and second orders of lens radial and tangential distortions should be considered when measuring larger complex objects. To correct the lens distortion for any point  $(x_d, y_d)$ , the equations of lens distortion correction are<sup>[11]</sup>

$$\begin{aligned} x_d &= x_u + k_1 x_u (x_u^2 + y_u^2) + k_2 x_u (x_u^2 + y_u^2)^2 \\ &\quad + p_1 (3x_u^2 + y_u^2) + 2p_2 x_u y_u, \\ y_d &= y_u + k_1 y_u (x_u^2 + y_u^2) + k_2 y_u (x_u^2 + y_u^2)^2 \\ &\quad + 2p_1 x_u y_u + p_2 (x_u^2 + 3y_u^2), \end{aligned} \quad (2)$$

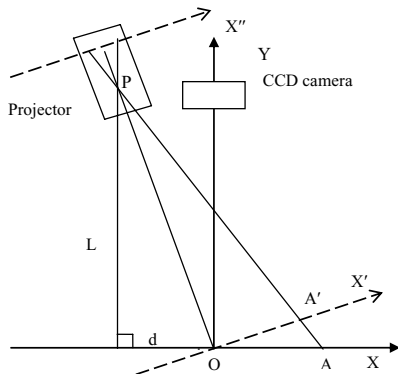


Fig. 1. Measurement system.

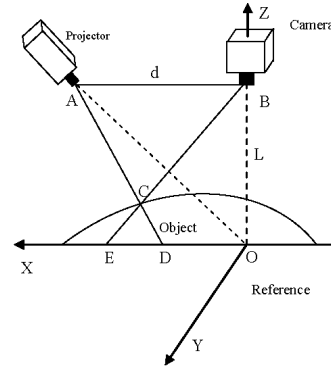


Fig. 2. Coordinate deviation correction.

where  $k_1$  and  $k_2$  are the first- and second-order coefficients of the lens radial distortion, respectively,  $p_1$  and  $p_2$  are the first- and second-order coefficients of the lens tangential distortion, respectively,  $(x_d, y_d)$  is the distortion image coordinate, and  $(x_u, y_u)$  is the ideal image coordinate. Here  $k_1$ ,  $k_2$ ,  $p_1$ , and  $p_2$  can be obtained by the camera calibration.

The 3D shape measurement model of large objects can be established after correcting image point displacement and lens distortion errors. The relationship between the pixel and length coordinates of the image coordinate system and the relationship between the length coordinate of the image coordinate system and the world coordinate system are shown as

$$\begin{bmatrix} u \\ v \\ 1 \end{bmatrix} = \begin{bmatrix} 1/u_x & 0 & u_0 \\ 0 & 1/u_y & v_0 \\ 0 & 0 & 1 \end{bmatrix} \begin{bmatrix} x_d \\ y_d \\ 1 \end{bmatrix}, \quad (3)$$

$$s \begin{bmatrix} x_u \\ y_u \\ 1 \end{bmatrix} = \begin{bmatrix} f' & 0 & 0 & 0 \\ 0 & f' & 0 & 0 \\ 0 & 0 & 1 & 0 \end{bmatrix} \begin{bmatrix} R & T \\ 0^T & 1 \end{bmatrix} \begin{bmatrix} X \\ Y \\ Z \\ 1 \end{bmatrix}. \quad (4)$$

The height  $h$  of the larger object can be calculated using Eq. (1).  $s$ ,  $u_0$ ,  $v_0$ ,  $u_x$ , and  $u_y$  are the camera internal parameters that can be obtained in advance by calibrating the camera.  $R$  and  $T$  are the unit orthogonal and translation matrices, respectively and  $f'$  is the focal length of the CCD camera. Assuming that the pixel coordinate of the image coordinate system is  $(u, v)$ , its corresponding length coordinate  $(x_d, y_d)$  can be obtained using Eq. (3).  $(x_u, y_u)$  can be obtained using Eq. (2), then the world coordinate  $(X, Y)$  can be solved using Eq. (4), where  $Z = 0$ . The world coordinate of the point is  $\left[ \left(1 - \frac{h}{L}\right)X, \left(1 - \frac{h}{L}\right)Y, h \right]$  after coordinate deviation correction is applied.

The sinusoidal grating fringe is on an oblique angle projected onto plane  $X$ , (Fig. 1).  $A'$  is the point on plane  $X'$  corresponding to point  $A$  on  $X$ . The fringe frequency on the reference plane is a constant value  $f$ ,  $OA = x$  and  $OA' = x'$  are supposed,  $op = (L^2 + d^2)^{1/2}$ .

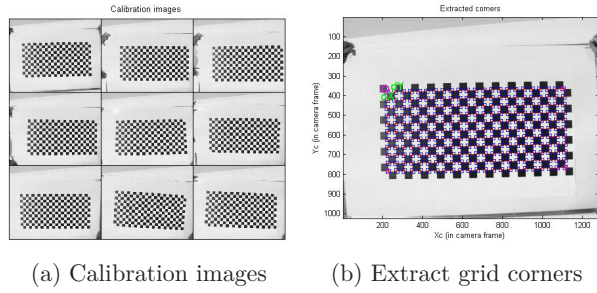


Fig. 3. Camera calibration process: (a) calibration images and (b) extract grid corners.

The relationship between the reference plane  $X$  and the virtual plane  $X'$  can be represented as<sup>[22]</sup>

$$x = \frac{op^2 x'}{L \cdot op - x' \cdot d}. \quad (5)$$

Using the  $N$ -step phase-shifting method, the grating fringe on the reference plane is moved by  $T/N$ , that is,  $x - T/N = [op^2 x' / (L \cdot op - x' \cdot d)]$  ( $T$  is the period of the grating fringe on the reference plane). Because  $A$  and  $A'$  are in the same optical path,  $\phi(x) = \phi(x')$  can be obtained.  $M$  is the magnification of the projector,  $x''$  is the coordinate on the projector plane corresponding to  $x'$ , and  $x' = Mx''$ . The  $N$ -step phase-shifting equation on the projector plane can be deduced as

$$\phi(x'') = \frac{2\pi f \cdot op^2 \cdot Mx''}{L \cdot op - Mx'' \cdot d} + 2\pi \frac{n}{N} \quad (n = 1, 2, 3 \dots N). \quad (6)$$

If the grating fringe phase on the projector plane is in accordance with Eq. (6), the constant cycle grating fringe can be obtained on the reference plane. The  $N$ -step phase-shifting algorithm can be described as

$$I_n(x, y) = a(x, y) + b(x, y) \cos[\phi(x, y) + 2\pi n/N], \quad (7)$$

where  $a(x, y)$  is the background light intensity,  $b(x, y)$  is the light intensity amplitude,  $n = 1, 2, 3, \dots, N$ , and  $\phi(x)$  is the wrapped phase that can be solved by<sup>[12]</sup>

$$\phi(x, y) = \tan^{-1} \frac{\sum_{n=1}^N I_n(x, y) \sin(2\pi n/N)}{\sum_{n=1}^N I_n(x, y) \cos(2\pi n/N)}, \quad (8)$$

and the wrapped phase  $\phi(x, y)$  ranges from  $-\pi$  to  $\pi$ .

The temporal phase unwrapping method can achieve phase unwrapping of larger complex objects. Using

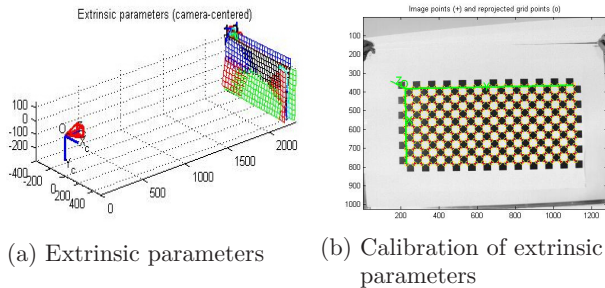


Fig. 4. Calibration of extrinsic parameters: (a) extrinsic parameters and (b) calibration of extrinsic parameters.

the  $N$ -step phase-shifting method based on the fringe cycle correction, the fringe frequencies on the reference plane change according to the rule  $2^i f$  ( $i = 0, 1, 2, \dots$ ). The grating fringes based on temporal phase unwrapping method are obtained.

The theory of the temporal phase unwrapping method is as follows:

Working out the wrapped phase  $\varphi_{f(i)}(m, n)$  of each frequency by adopting Eq. (8), the absolute phase  $\Phi_{f(0)}(m, n)$  can be solved by  $\varphi_{f(0)}(m, n)$  ( $i = 0$ ). The absolute phase  $\Phi_{f(i)}(m, n)$  can be deduced from  $\Phi_{f(i)}(m, n) = \varphi_{f(i)}(m, n) + 2\pi \times O_{f(i-1)}(m, n)$  ( $i = 1, 2, 3, \dots$ ).

The function  $O_{f(i-1)}(m, n)$  can be expressed as

$$o_{f(i-1)}(m, n) = \text{INT} \left( \frac{\Phi_{f(i-1)}(m, n) \times k - \varphi_{f(i)}(m, n)}{2\pi} \right), \quad (9)$$

where  $\text{INT} (*)$  means the nearest integer of  $*$  and  $k$  is the increase index of the frequency; here,  $k = 2$ .

The measurement system is shown in Fig. 1. It comprises a Samsung projector and a CCD camera (DH-HV1351UM) with a focal length of 14 mm. The resolution of the projector is  $1024 \times 768$  and the resolution of the CCD camera is  $1024 \times 768$ . The fringe patterns are on an oblique angle projected onto the measured object and reference plane, respectively. The images are captured by the CCD camera.

Standard blocks are used to calibrate the parameters  $L$  and  $d$  after vertical and parallel calibration of the system.  $L$  is  $210.004 \pm 0.022$  cm and  $d$  is  $115.002 \pm 0.017$  cm.  $M$  is obtained through a simple experiment and  $M$  is  $3.101 \pm 0.008$ .  $f$  can be set to a reasonable value depending on requirements.  $L$ ,  $d$ ,  $M$ , and  $f$  can be set from the input interface of grating generating software. Subsequently, the desired grating can be achieved. The internal and external parameters are calibrated using Zhang's 2D plane template method<sup>[23]</sup>, taking into account the lens distortion and coordinate deviation. The experiments performed are discussed below.

The calibration images and the process of extracting grid corners are shown in Fig. 3. Figure 4 shows the calibration of extrinsic parameters. The calibration results of the intrinsic and extrinsic parameters are presented in Table 1.

A slab ( $125 \times 2.45 \times 2.45$  cm) is used in comparative experiments to prove the availability of the proposed method. Sinusoidal fringes are used to measure the slab by employing the temporal phase unwrapping method based on uncorrected and corrected fringe cycles, respectively. Figure 5 shows  $270^\circ$  phase-shifting images of the reference plane. Figure 6 shows  $270^\circ$  phase-shifting images of the slab. Figure 7 depicts the absolute phase difference.

The absolute phase difference can be obtained utilizing the temporal phase unwrapping method. The height of the slab can be solved by Eq. (1). Finally, the world coordinates of the slab can be obtained using the 3D shape measurement model of larger objects. Figure 8

**Table 1.** Camera Calibration Results of the Intrinsic and Extrinsic Parameters

Intrinsic Parameters	Focal Length	Principal Point	Lens Distortion	Pixel Error
	$fx = 2570.8556$	$u_0 = 634.4821$	$k_1 = -0.34719$	$err\_x = 0.25844$
	$fy = 2570.7478$	$v_0 = 525.3569$	$k_2 = 0.17140$	$err\_y = 0.29377$
			$p_1 = -0.00105$	
			$p_2 = 0.00024$	
Extrinsic Parameters	Translation Vector	Rotation Matrix	Pixel Error	
	$T_{11} = -376.01206$	$r_{11} = 0.02037$	$err\_x = 0.20314$	
		$r_{12} = 0.99979$		
		$r_{13} = -0.00094$		
	$T_{21} = -130.34975$	$r_{21} = 0.99931$		
		$r_{22} = -0.02039$		
		$r_{23} = -0.03106$		
	$T_{31} = 2313.74960$	$r_{31} = -0.03107$	$err\_y = 0.23772$	
		$r_{32} = -0.00031$		
		$r_{33} = -0.99952$		

shows the height of the slab. Figure 9 shows the height error of the slab.

To correct the camera lens distortion, the calibrated lens distortion coefficients  $k_1$ ,  $k_2$ ,  $p_1$ ,  $p_2$ , and the distortion image coordinate  $(x_d, y_d)$  are used to solve the nonlinear Eq. (2) to obtain the ideal image coordinate  $(x_u, y_u)$ . The Newton iteration method is used to solve Eq. (2). The specific steps are as follows<sup>[24]</sup>:

1) Assuming that  $(x_u, y_u)$  is the old variable and  $(x_{u0}, y_{u0})$  is the new variable. Equation (2) can be expressed as

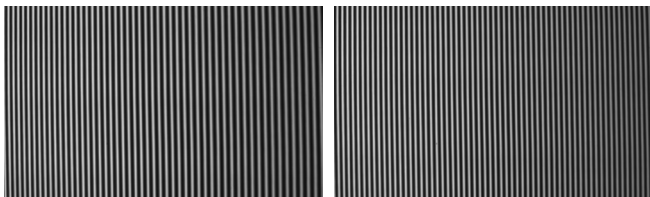
$$\begin{cases} f_1(x_u, y_u) = f_1 = x_u + k_1 x_u (x_u^2 + y_u^2) + k_2 y_u (x_u^2 + y_u^2)^2 \\ \quad + p_1 (3x_u^2 + y_u^2) + 2p_2 x_u y_u - x_d, \\ f_2(x_u, y_u) = f_2 = y_u + k_1 y_u (x_u^2 + y_u^2) + k_2 x_u (x_u^2 + y_u^2)^2 \\ \quad + 2p_1 x_u y_u + p_2 (x_u^2 + 3y_u^2) - y_d. \end{cases} \quad (10)$$

2) The following iterative formula is established:

$$\begin{cases} x_{u1} = x_u - \frac{(f_1 f_{2y_u} - f_2 f_{1y_u})}{(f_{1x_u} f_{2y_u} - f_{1y_u} f_{2x_u})}, \\ y_{u1} = y_u - \frac{(f_2 f_{1x_u} - f_1 f_{2x_u})}{(f_{1x_u} f_{2y_u} - f_{1y_u} f_{2x_u})}, \end{cases} \quad (11)$$

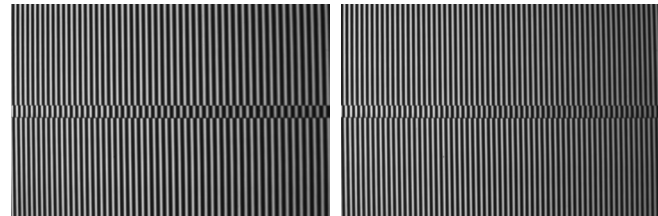
where  $f_{1x_u}$ ,  $f_{1y_u}$ ,  $f_{2x_u}$ , and  $f_{2y_u}$  are the first-order partial derivatives of Eq. (10),  $f_1(x_u, y_u)$ , and  $f_2(x_u, y_u)$ . The iteration formula can be described as

$$\begin{cases} x_{uk} = x_{u(k-1)} - (f_1 f_{2y_u} - f_2 f_{1y_u}) / (f_{1x_u} f_{2y_u} - f_{1y_u} f_{2x_u}), \\ y_{uk} = y_{u(k-1)} - (f_2 f_{1x_u} - f_1 f_{2x_u}) / (f_{1x_u} f_{2y_u} - f_{1y_u} f_{2x_u}), \end{cases} \quad (k = 1, 2, 3 \dots N), \quad (12)$$



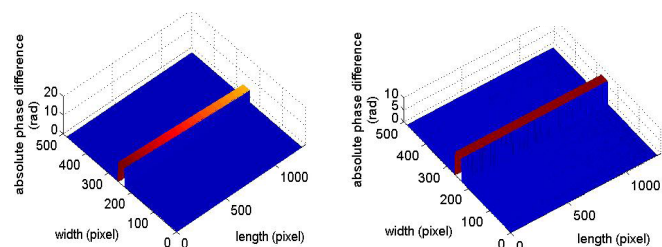
(a) Uncorrected fringe cycle (b) Corrected fringe cycle

Fig. 5. 270° phase-shifting images of the reference plane based on (a) uncorrected and (b) corrected fringe cycles, respectively.



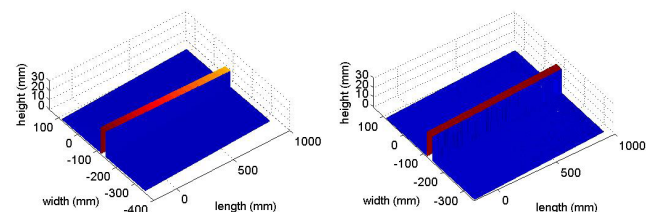
(a) Uncorrected fringe cycle (b) Corrected fringe cycle

Fig. 6. 270° phase-shifting images of the slab based on (a) uncorrected and (b) corrected fringe cycles, respectively.



(a) Uncorrected fringe cycle (b) Corrected fringe cycle

Fig. 7. Absolute phase difference based on (a) uncorrected and (b) corrected fringe cycles, respectively.



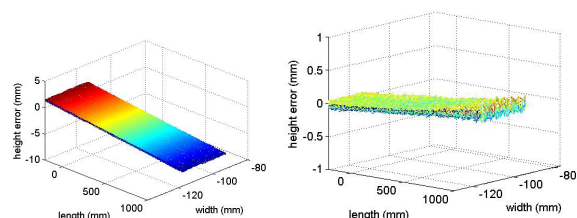
(a) Uncorrected fringe cycle (b) Corrected fringe cycle

Fig. 8. Height of slab based on (a) uncorrected and (b) corrected fringe cycles, respectively.

where  $(x_{uk}, y_{uk})$  is the  $k$  times' iteration variable of the initial variable  $(x_{u0}, y_{u0})$ .  $(x_{uk}, y_{uk})$  is then substituted into Eq. (12) to acquire the new equations  $f_1, f_2, f_{1x_u}, f_{1y_u}, f_{2x_u}$ , and  $f_{2y_u}$  for the next iteration.

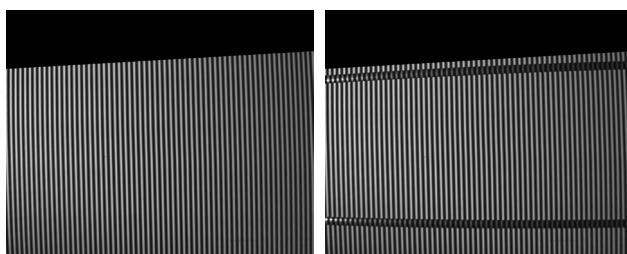
3) The iteration is ceased when the absolute values of  $f_1(x_u, y_u)$  and  $f_2(x_u, y_u)$  are less than  $10^{-6}$ ; the final value of  $(x_{uk}, y_{uk})$  is the ideal image coordinate.

Two long straight slabs (length is approximately 140 cm) are used for the lens distortion correction experiment. Figure 10(a) shows the phase-shifting image of the reference plane. Two straight slabs are placed on the upper and lower edges (Fig. 10(b)), given that the lens distortion at the edge of the view field is evident. Figures 10(c) and (d) show the absolute phase difference of plane and straight slabs, respectively. Figures 11(a) and (b) show the original and lens distortion-corrected 3D measurement results of the straight slabs, respectively. Figure 11(a) shows that the straight slabs bend to a certain degree because of the influence of lens distortion.

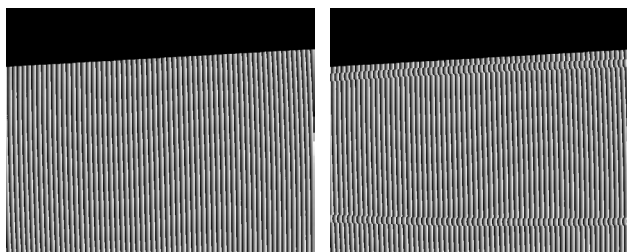


(a) Uncorrected fringe cycle (b) Corrected fringe cycle

Fig. 9. Height error of the slab based on (a) uncorrected and (b) corrected fringe cycles, respectively.

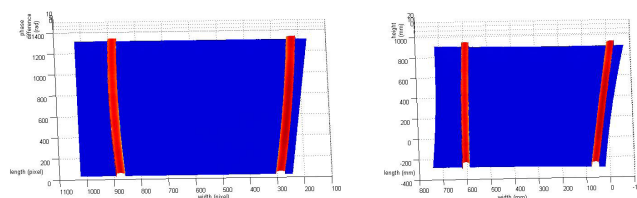


(a) Reference plane (b) Long straight slab



(c) The wrapped phase of the reference plane (d) The wrapped phase of long straight slab

Fig. 10. Phase-shifting and the wrapped phase images: (a) reference plane, (b) long straight slab, (c) wrapped phase of the reference plane, and (d) wrapped phase of long straight slab.

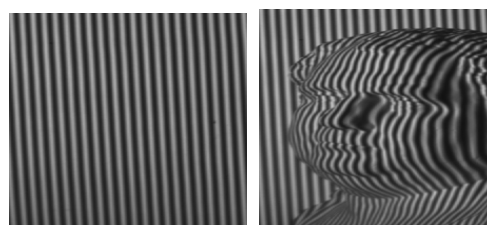


(a) Distortion uncorrected (b) Distortion corrected

Fig. 11. Long straight slabs 3D measurement results with lens (a) distortion uncorrected and (b) distortion corrected.

However, long straight slabs have been well recovered after lens distortion correction (Fig. 11(b)). These experimental results demonstrate that the proposed lens distortion correction model has effective performance.

A large complex plaster statue (45×30×65 cm) is measured to illustrate the effectiveness of the proposed method further. Figure 12 shows the 270° phase-shifting images of the reference plane and the plaster statue based on the fringe cycle correction, respectively. The



(a) Reference plane (b) Plaster statue

Fig. 12. 270° phase-shifting images of the (a) reference plane and (b) plaster statue based on the fringe cycle correction.

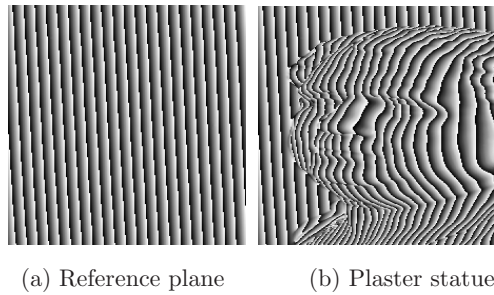


Fig. 13. Wrapped phase of the (a) reference plane and (b) plaster statue based on the fringe cycle correction.

wrapped phase is shown in Fig. 13. The 3D shape of the plaster statue is presented in Fig. 14.

The height error without fringe cycle correction increases along the  $x$ -axis direction (Fig. 8(a)). The RMS error is 3.01 mm compared with that of the standard 3D shape of the slab. The height error is 3.61 mm at (500 and 243 pixel), and the relative error is approximately 14.4%. The height of the slab using the proposed method is almost consistent with the actual height (Fig. 8(b)), and its RMS error is 0.20 mm. The height error of the slab is 0.22 mm at (500 and 243 pixel) and the relative error is less than 0.88%; the height error is significantly reduced (Fig. 9). Figure 11 shows that the lens distortion correction method proposed in this letter can effectively realize lens distortion correction. Therefore, the measurement accuracy of the proposed method is significantly improved.

The proposed method presents the solution to obtain accurate and stable 3D shapes of large complex objects. Figures 8 and 14 show that the proposed method can measure a large complex plaster statue well, with eyes and nose that are clearly discernible. The RMS error is 0.25 mm compared with that of the standard 3D shape of the plaster statue.

In conclusion, we propose a temporal phase unwrapping method based on the fringe cycle correction. The

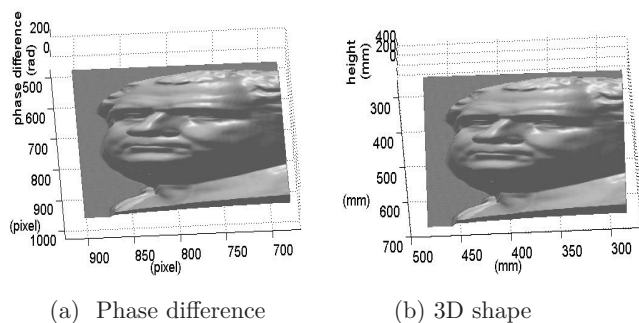


Fig. 14(a) Phase difference and (b) 3D shape of the measured plaster statue.

method generates the uniform sinusoidal fringes on the reference plane by producing the nonuniform sinusoidal fringes on the projection plane and can reduce the error, thereby improving measurement accuracy. Experimental results demonstrate that the proposed method can solve the problem of the fringe cycle broadening on the reference plane and correct lens distortion issues. Thus, the 3D shapes of larger complex objects can be measured accurately using the proposed method.

This work was supported by the National Natural Science Foundation of China (No. 51365045), the Natural Science Foundation of Jiangxi Province (No. 20122BAB202012), the Aviation Science Fund (No. 2013ZE56013), and the Education Department of Jiangxi Province (No. GJJ13522).

## References

1. M. Takeda and K. Mutoh, *Appl. Opt.* **22**, 3977 (1983).
2. G. Sansoni, M. Carocci, and R. Rodella, *IEEE Trans. Instrum. Meas.* **49**, 628 (2000).
3. Z. Wang and H. Du, *Opt. Express* **14**, 12122 (2006).
4. L. Chen and C. Quan, *Opt. Lett.* **30**, 2101 (2005).
5. B. Rajoub, M. Lalor, D. Burton, and S. Karout, *J. Opt. A: Pure Appl. Opt.* **9**, 66 (2007).
6. S. Luis, L. Esteban, S. Javier, V. Garcia, and M. Servin, *Opt. Eng.* **42**, 3307 (2003).
7. Y. Wu, Y. Cao, and Y. Xiao, *Chin. J. Lasers* **38**, 09080091 (2011).
8. Z. Zhang, C. Towers, and D. Towers, *Appl. Opt.* **46**, 6113 (2007).
9. V. Cheng, R. Yang, C. Hui, and Y. Chen, *Opt. Eng.* **47**, 050503 (2008).
10. Y. Hao, Y. Zhang, and D. Li, *Acta Opt. Sin.* **20**, 376 (2000).
11. J. Li and D. Zhang, *Opt. Eng.* **50**, 023601 (2011).
12. B. Pan, Q. Kemao, L. Huang, and A. Asundi, *Opt. Lett.* **34**, 416 (2009).
13. H. Cui, W. Liao, N. Dai, and X. Cheng, *Chin. Opt. Lett.* **10**, 031201 (2012).
14. H. Guo, H. He, Y. Yu, and M. Chen, *Opt. Eng.* **44**, 033603 (2005).
15. X. Chen, J. Xi, J. Ye, and S. Jin, *Opt. Laser Eng.* **47**, 310 (2009).
16. Z. Wei and G. Zhang, *Opt. Laser Eng.* **43**, 1167 (2005).
17. F. Zhou, Y. Wang, Y. Cui, and H. Tan, *Chin. Opt. Lett.* **10**, 021003 (2012).
18. Q. Zhang, X. Su, L. Xiang, and X. Sun, *Opt. Laser Eng.* **50**, 574 (2012).
19. K. Liu, Y. Wang, D. Lau, Q. Hao, and L. Hassebrook, *Opt. Express* **18**, 5229 (2010).
20. R. Lu and Y. Li, *Sens. Actuators A: Phys.* **116**, 384 (2004).
21. Y. Yin, X. Peng, X. Liu, A. Li, and X. Qu, *Opt. Commun.* **285**, 2048 (2012).
22. Y. Fu and Q. Luo, *Opt. Express* **19**, 21739 (2011).
23. Z. Zhang, in *Proceedings of IEEE Transactions on Pattern Analysis and Machine Intelligence* **22** (2000).
24. C. Ninomiya, *Math. Comput.* **24**, 391 (1970).